JNS SPINE

LABORATORY INVESTIGATION

**J Neurosurg Spine** 38:662–672, 2023

# Can semirigid fixation of the rostral instrumented segments prevent proximal junctional kyphosis in the case of long thoracolumbar fusions? A finite element study

***Mate Turbucz, MSc,[1,2] Jennifer Fayad, MSc,[1,3] Agoston J. Pokorni, MSc,[1,2] Peter P. Varga, MD,[4] Peter E. Eltes, MD, PhD,[1,5] and Aron Lazary, MD, PhD[1,4,5]**

[1]In Silico Biomechanics Laboratory, National Center for Spinal Disorders, Buda Health Center, Budapest; [2]School of PhD Studies, Semmelweis University, Budapest, Hungary; [3]Department of Industrial Engineering, Alma Mater Studiorum, University of Bologna, Italy; [4]National Center for Spinal Disorders, Buda Health Center, Budapest; and [5]Department of Spine Surgery, Department of Orthopaedics, Semmelweis University, Budapest, Hungary

**OBJECTIVE** Proximal junctional kyphosis (PJK) is a relatively common complication following long instrumented posterior spinal fusion. Although several risk factors have been identified in the literature, previous biomechanical studies suggest that one of the leading causes is the sudden change in mobility between the instrumented and noninstrumented segments. The current study aims to assess the biomechanical effect of 1 rigid and 2 semirigid fixation techniques (SFTs) on developing PJK.

**METHODS** Four T7–L5 finite element (FE) models were developed: 1) intact spine; 2) 5.5-mm titanium rod from T8 to L5 (titanium rod fixation [TRF]); 3) multiple rods from T8 to T9 connected with titanium rod from T9 to L5 (multiple-rod fixation [MRF]); and 4) polyetheretherketone rod from T8 to T9 connected with titanium rod from T9 to L5 (PEEK rod fixation [PRF]). A modified multidirectional hybrid test protocol was used. First, a pure bending moment of 5 Nm was applied to measure the intervertebral rotation angles. Second, the TRF technique's displacement from the first loading step was applied to the instrumented FE models to compare the pedicle screw stress values in the upper instrumented vertebra (UIV).

**RESULTS** In the load-controlled step, at the upper instrumented segment, the intervertebral rotation values relative to TRF increased by 46.8% and 99.2% for flexion, by 43.2% and 87.7% for extension, by 90.1% and 137% for lateral bending, and by 407.1% and 585.2% for axial rotation, in the case of MRF and PRF, respectively. In the displacement-controlled step, maximum pedicle screw stress values at the UIV level were highest in the case of TRF (37.26 MPa, 42.13 MPa, 44.4 MPa, and 44.59 MPa for flexion, extension, lateral bending, and axial rotation, respectively). Compared to TRF, in the case of MRF and PRF, the screw stress values were reduced by 17.3% and 27.7% for flexion, by 26.6% and 36.7% for extension, by 6.8% and 34.3% for lateral bending, and by 49.1% and 59.8% for axial rotation, respectively.

**CONCLUSIONS** FE analysis has shown that the SFTs increase the mobility at the upper instrumented segment and therefore provide a more gradual transition in motion between the instrumented and rostral noninstrumented segments of the spine. In addition, SFTs decrease the screw loads at the UIV level and hence could help reduce the risk for PJK. However, further investigations are recommended to evaluate the long-term clinical usefulness of these techniques.

https://thejns.org/doi/abs/10.3171/2023.1.SPINE22931

**KEYWORDS** adult spinal deformity; proximal junctional kyphosis; spine surgery; biomechanics; finite element analysis; thoracolumbar; semirigid fixation; rostral instrumented segment; thoracic

In recent years, the upward shift in age demographics has led to a significant increase in the prevalence of adult spinal deformity.[1] In treating patients with adult spinal deformity, the application of surgical fixation techniques has grown significantly. However, these surgical techniques remain a cause for concern and must be carefully considered because they are associated with increased revision and complication rates.[1] Proximal junctional kyphosis (PJK) is a complication with an incidence rate ranging from 17% to 39% within 2 years of surgery.[2]

**ABBREVIATIONS** AF = annulus fibrosus; FE = finite element; GS = ground substance; HD = Hausdorff distance; IVD = intervertebral disc; IVR = intervertebral rotation; MRF = multiple-rod fixation; NP = nucleus pulposus; PEEK = polyetheretherketone; PJK = proximal junctional kyphosis; PRF = PEEK rod fixation; ROM = range of motion; SFT = semirigid fixation technique; SK = segmental kyphosis; TPH = transverse process hook; TRF = titanium rod fixation; UIV = upper instrumented vertebra.

**SUBMITTED** August 17, 2022. **ACCEPTED** January 11, 2023.

**INCLUDE WHEN CITING** Published online March 3, 2023; DOI: 10.3171/2023.1.SPINE22931.

* M.T. and J.F. contributed equally to this work.



© 2023 The authors, CC BY-NC-ND 4.0 (http://creativecommons.org/licenses/by-nc-nd/4.0/)

Unauthenticated | Downloaded 08/17/23 07:42 PM UTC

PJK is an abnormal kyphotic deformity affecting the vertebral components proximal to the upper instrumented vertebra (UIV). PJK is described by the segmental kyphosis (SK) defined by the proximal junctional Cobb angle measured between the UIV and the vertebra 2 levels rostral to the UIV (UIV+2).[3] PJK occurs if the SK between the UIV and UIV+2 is at least 10° or if the SK increases by at least 10° after surgery.[3] In more severe cases, PJK includes vertebral subluxation, vertebral body fracture, implant failure, damage to the posterior ligament complex, or adjacent-level degeneration, thus requiring revision surgery.[4]

Various patient-specific risk factors have been linked to PJK, such as older age, higher body mass index, lower bone mineral density, and presence of comorbidities.[5] Surgery-related risk factors have also been identified, such as the position of the UIV, given that PJK is more likely to occur at the lower thoracic and the thoracolumbar regions.[5] Furthermore, a high construct rigidity, a high degree of corrected deformity, and the number of fused vertebrae were also considered surgical risk factors.[6] In addition, the quantitative GAP (Global Alignment and Proportion) score was found to be an efficient tool for predicting mechanical complications such as PJK.[7]

Besides these, the sudden change in rigidity between the instrumented and noninstrumented segments was also identified as a contributing factor to the onset of PJK.[8] To address this problem, various semirigid fixation techniques (SFTs)[8] were introduced in the literature, such as transverse process hooks (TPHs),[9] transition rods with a smaller diameter,[10] or the use of polyetheretherketone (PEEK) at the rostral end instead of metallic alloys.[11] The purpose of such implants is to provide a more gradual transition to normal motion at the UIV level following long instrumented posterior spinal fusion, thereby reducing the probability of developing PJK.[12]

Previously, various in vitro experiments were performed to investigate the effect of different spinal constructs on the development of PJK. Thawrani et al. analyzed the biomechanical effect of placing TPHs at the UIV level[9] and found that TPHs can provide a more gradual transition in motion than more rigid constructs and thus reduce the incidence of postoperative PJK.[9] Viswanathan et al. published their findings that the SFTs could effectively extend the transition zone and reduce peak stress at the UIV level of long-segment thoracolumbar fixations.[13] Doodkorte et al. analyzed different SFTs, such as TPHs, and the use of sublaminar tapes at the rostral end of the construct.[12] They found a more beneficial transition in mobility at the junctional levels in all semirigid constructs compared to the conventional pedicle screw fixation.[12]

Besides the in vitro measurements, finite element (FE) analyses were also used to understand the biomechanical background of PJK. Bess et al. evaluated the effect of posterior anchored polyethylene tethers and concluded that the tethers provided a more gradual transition in range of motion (ROM) and reduced the load in the posterior ligament complex and in the pedicle screws at the UIV level.[14] Zhang et al. investigated the application of PEEK rods and found that the risk of PJK is lower in the case of SFTs in which PEEK rods are used.[15] As pointed out, these studies agree that the biomechanical assessment of the instrumented spinal segments may help predict and prevent postoperative PJK.

In the current study, 2 different SFTs were investigated and compared to the conventionally used titanium rod fixation (TRF) technique. The multiple-rod fixation (MRF) technique, based on the arrangement of thinner titanium rods in a shield pattern, was introduced by Farkas and Varga in 2002.[16] MRF aims to improve angular mobility while maintaining the stability resulting from the titanium material.[16] The PEEK rod fixation (PRF) technique consists of PEEK material at the rostral end of the construct to decrease its rigidity. Among the previous in vitro and in silico studies of SFTs, the MRF technique has not been previously investigated in relation to PJK. Furthermore, the effect of PEEK material at the rostral end of the construct on mobility and load distribution in long posterior spinal fixations has not been previously analyzed.

The present study investigates the biomechanical impact of MRF and PRF by comparing their effect on developing PJK after long thoracolumbar fusion. The mobility related to the SFT was evaluated through the intervertebral rotation (IVR) values, whereas the load at the UIV level was characterized by the maximum stress values on the implant-bone surface and the stress distribution at the UIV level.

## Methods

### Development of the Intact T7–L5 Model

The nonlinear FE model of the T7–L5 spine was developed based on CT scans (Hitachi Presto; Hitachi Medical Corp.) of the thoracolumbar and lumbar regions (slice thickness 0.625 mm) obtained in a healthy 24-year-old man (Fig. 1A). The CT data of the patient were obtained from the hospital's PACS in DICOM extension, followed by an anonymization process performed using the Clinical Trial Processor software (Radiological Society of North America).[17] Using the 2D images of the CT scans, a threshold-based segmentation was used to obtain the 3D geometrical representation of the thoracolumbar and lumbar spine segment in the Mimics software (Mimics Research, Mimics Innovation Suite version 23.0; Materialise). Subsequently, the triangulated surface meshes were imported into 3-Matic software (Mimics Research, Mimics Innovation Suite version 21.0; Materialise) in STL format. Both the thoracolumbar (T7–L1) and lumbar (L1–5) regions included the first lumbar vertebra, which served as a basis for the n-point rigid surface registration, creating the T7–L5 spine model in a common reference system (Fig. 1B). The quality of the registration and alignment was checked by calculating the Hausdorff distance (HD) with MeshLab software (MeshLab version 1.3.2; Metro Tool, Visual Computing Lab) (Fig. 1C).[18]

The aligned T7–L5 spine model was then imported into HyperWorks software (Altair Engineering, Inc.), where the final geometry model was constructed. The vertebrae were divided into the 1-mm thin cortical shell, the cancellous core, the 0.5-mm thin vertebral endplates, and the posterior elements.[19,20] The bony components of the vertebral bodies were meshed with 1-mm linear tetrahedral elements. Facet joints were modeled as 0.25-mm thin cartilaginous



Unauthenticated | Downloaded 08/17/23 07:42 PM UTC

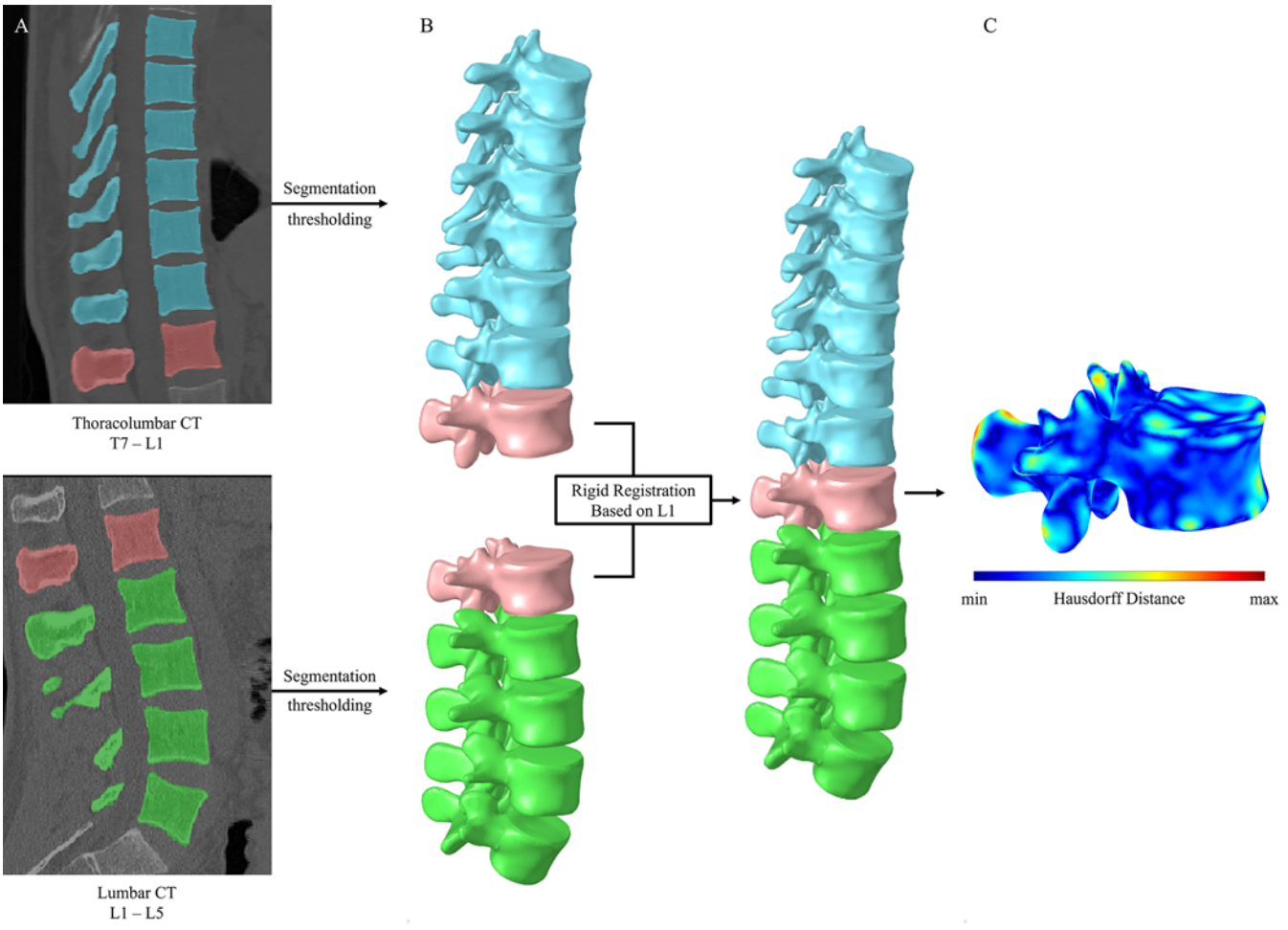


**FIG. 1.** Overview of the modeling process. **A:** The segmentation of the thoracolumbar and lumbar regions. **B:** Rigid surface registration of the generated 3D thoracolumbar and lumbar models and the aligned T7–L5 geometry model. **C:** Visualization of the HD between the 2 L1 geometries acquired from the thoracolumbar and lumbar CT scans. Figure is available in color online only.

layers with an initial gap of 0.5 mm between the adjacent surfaces using wedge elements.[21,22] The geometry of the intervertebral discs (IVDs) was created based on anatomical descriptions in which 8-node hexahedral elements were used.[23] The IVD included the 0.5-mm thin cartilaginous endplate, the nucleus pulposus (NP), and the annulus fibrosus (AF) built from 6 concentric layers around the NP.[24] AF was modeled as composite-like material consisting of the annulus ground substance (GS) and the annulus fibers. The fibers were modeled with 2-node truss elements at an alternating angle of 30°/150° to the axial plane of the IVD.[25] The fiber's cross-sectional area values were acquired from the fiber's volume ratio to the GS, which varied from the inner to the outer layers: 5% at the innermost and 23% at the outermost layer.[26] The NP accounted for 45% of the IVD volume and was shifted posteriorly, agreeing with the general anatomical descriptions.[23,27] All 7 major ligaments were included in the current study—anterior longitudinal ligament, posterior longitudinal ligament, interspinous ligament, supraspinous ligament, capsular ligaments, ligamentum flavum, and intertransverse ligament. These were modeled using uniaxial spring elements.[28]

## Material Properties

The current study adopted homogeneous and isotropic material properties for all anatomical regions. Linear elastic material properties were used for the cortical and cancellous bone, the vertebral and cartilaginous endplates, and the posterior elements.[29–32] In the case of the facet joints, the Neo-Hooke hyperelastic material property was applied.[32] For the annulus GS and the NP, a 2-parameter Mooney-Rivlin formulation was used to simulate their incompressible behavior.[33] Given that the inner layers of the IVD are less stiff than the outer layers, the annulus fibers were weighted by scalar factors obtained for each layer (innermost layer: 0.65; outermost layer: 1).[34] Ligaments were modeled with tension-only nonlinear stress-strain curves reported in the literature.[28] The material properties and the element types are summarized in Table 1.

## Model Calibration and Validation

The material properties of the IVDs in the thoracolumbar region (T7–L1) were calibrated to approximate the IVR values measured in vitro. Two scalar calibration



Unauthenticated | Downloaded 08/17/23 07:42 PM UTC

**TABLE 1. Summary of the applied material properties and element types of the current study**

| Region | Element Type | Material Properties | Reference |
|---|---|---|---|
| Cortical bone | C3D4 | E = 10,000; ν = 0.3 | Rohlmann et al., 2006[30] |
| Trabecular bone | C3D4 | E = 100; ν = 0.2 | Shirazi-Adl et al., 1986[31] |
| Posterior elements | C3D4 | E = 3,500; ν = 0.25 | Shirazi-Adl et al., 1986[31] |
| Vertebral endplate | C3D4 | E = 1,200; ν = 0.29 | Li et al., 2015[29] |
| Cartilaginous endplate | C3D6, C3D8 | E = 23.8; ν = 0.42 | Finley et al., 2018[32] |
| Facet cartilage* | C3D6 | C10 = 5.36; D1 = 0.04 | Finley et al., 2018[32] |
| NP† | C3D8H | C10 = 0.12; C01 = 0.03 | Schmidt et al., 2007[33] |
| AF GS† | C3D8H | Lumbar region: C10 = 0.18; C01 = 0.045; thoracic region: calibrated stress-strain relationship | Schmidt et al., 2006;[34] Schmidt et al., 2007[33] |
| AF fibers | T3D2 | Lumbar region: weighted nonlinear stress-strain relationship (CSA values calculated at each layer); thoracic region: calibrated stress-strain relationship | Shirazi-Adl et al., 1986;[31] Schmidt et al., 2006;[34] Lu et al., 2013[26] |
| Ligaments | SPRINGA | Nonlinear stress-strain relationship | Rohlmann et al., 2006[28] |
| Titanium | C3D4 | E = 110,000; ν = 0.3 | Li et al., 2015[29] |
| PEEK | C3D4 | E = 3,600; ν = 0.3 | Li et al., 2015[29] |

C01, C10, D1 = material parameters; CSA = cross-sectional area; E = Young's modulus (in MPa); ν = Poisson's ratio.
* Neo-Hooke hyperelastic model.
† Mooney-Rivlin hyperelastic model.

parameters were introduced: $\lambda_{GS}$ was used to calibrate the material of the annulus GS, with extreme values of 0.0025 and 238, which correspond to the physiological limits of the GS material; $\lambda_{fiber}$ was used as a weighting factor for the stress-strain relationship of the fibers and could take values between 0.3 and 2.[34]

To validate the T7–L5 intact spine model, pure bending moments were applied in the 3 anatomical planes to mimic flexion-extension, lateral bending, and axial rotation. Multiple FE models were created and loaded at the most rostral endplate, whereas the most caudal endplate was fixed in all degrees of freedom.[35] Calculated IVR values of the FE models were compared with the available in vitro data from the literature.[36–38]

### Development of the Spinal Fixation Models

To investigate the biomechanical effect of different SFTs on the onset of PJK, in addition to the intact model (Fig. 2A), 1 rigid and 2 semirigid models were developed as follows. 1) TRF—model with posterior fusion of the spine from T8 to L5 performed using bilateral pedicle screws and 5.5-mm-diameter titanium rods (Fig. 2C). 2) PRF—model with 5.5-mm-diameter PEEK rods between T8 and T9 combined with posterior stabilization of the spine from T9 to L5 achieved using bilateral pedicle screws and 5.5-mm-diameter titanium rods. A rod connector system was placed to connect the titanium and PEEK rods (Fig. 2B). 3) MRF—model with five 1.9-mm-diameter titanium rods between T8 and T9 combined with posterior fusion of the spine from T9 to L5 performed using bilateral pedicle screws and 5.5-mm-diameter titanium rods. A rod connector system was placed to connect the titanium and the multiple titanium rods (Fig. 2D).

### Load and Boundary Conditions

For all FE models, the loading was applied at the superior endplate of T7, whereas the inferior endplate of L5 was fixed in all degrees of freedom. For a proper biomechanical evaluation of adjacent-segment effects, a modified multidirectional hybrid test protocol has been applied in this study, consisting of 2 consecutive loading steps.[39] 1) Load-controlled step: the intact T7–L5 and the instrumented FE models were loaded with 5-Nm pure bending moment in the anatomical planes to simulate flexion-extension, lateral bending, and axial rotation.[14] IVR values of the intact spine and the spinal fixation techniques were measured. Then, the IVR values of the intact spine were used to normalize the results of the 3 instrumented FE models. For symmetrical load cases, such as lateral bending and axial rotation, the right- and left-side values were averaged. 2) Displacement-controlled step: for a physiologically realistic comparison, the displacement of the TRF technique obtained from the first loading step was used as an input for the second loading step. The maximum von Mises stress values in the pedicle screws and the stress distribution at the UIV level were analyzed. The maximum stress values for lateral bending and axial rotation were averaged similarly to the first step.

## Results

### Hausdorff Distance

HD values were calculated to assess the quality of the alignment and registration. HD values were visualized between the segmented thoracolumbar-based L1 and the lumbar-based L1 vertebrae (Fig. 1C). Minimum and maximum HD values were 0 mm and 1.37 mm (mean 0.15 mm, root mean square 0.2), respectively.

### Model Calibration and Validation

Weighting factor values for the annulus GS were between 0.28 and 0.5, and for the fibers the values were between 0.4 and 0.5. In more detail, the weighting factors obtained from the calibration process are given in the



Unauthenticated | Downloaded 08/17/23 07:42 PM UTC

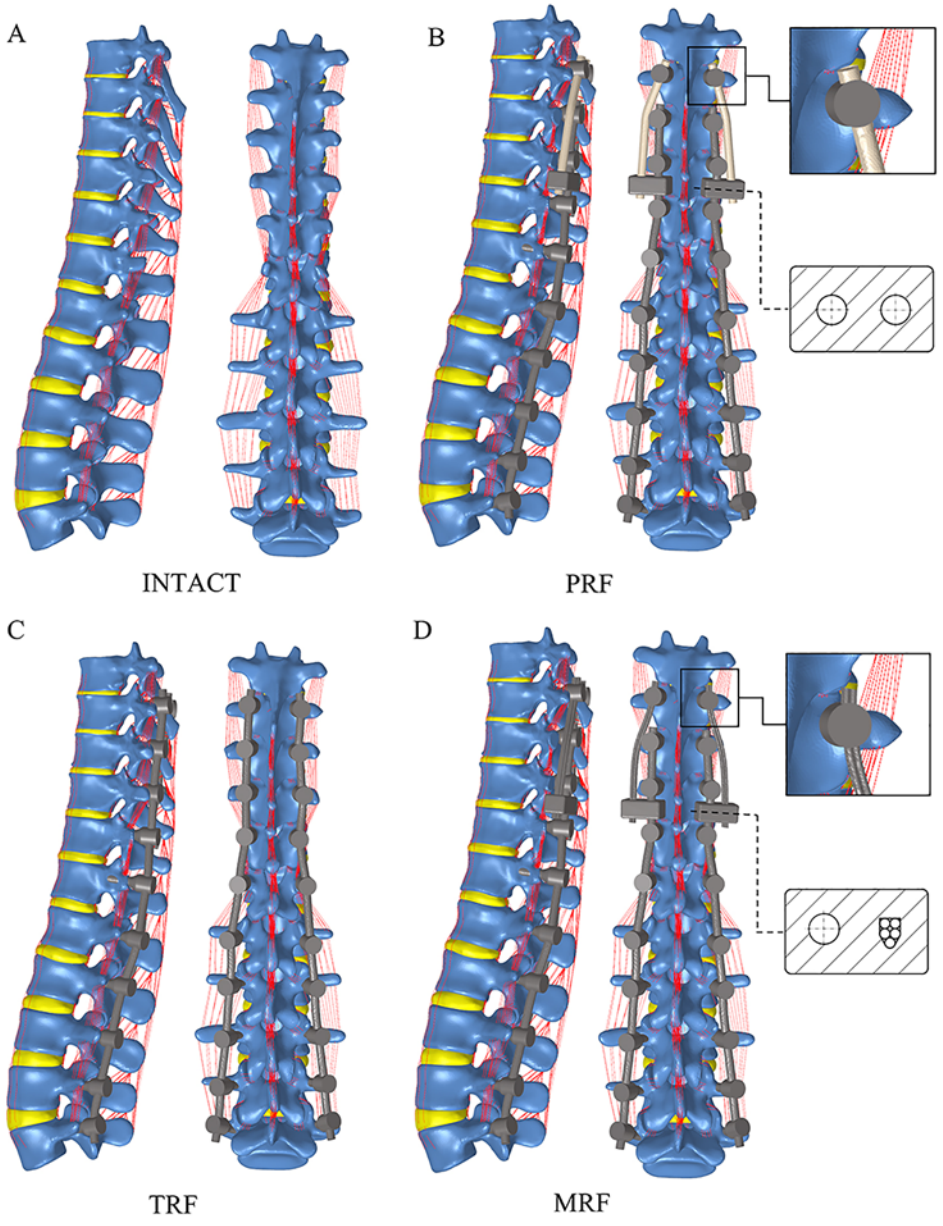


**FIG. 2.** The analyzed spinal fixation techniques in lateral and posterior views. **A:** The intact T7–L5 model. **B:** The PRF model. **C:** The TRF model. **D:** The MRF model. Figure is available in color online only.

online appendix, Supplementary Table 1. The IVR results of the model calibration were within the range of available in vitro measurements for all load cases, except at the T9–10 level for lateral bending (Supplementary Fig. 1–3). In flexion-extension and axial rotation, the predicted values showed good agreement with the in vitro midvalues, whereas in lateral bending, the predictions of the FE model slightly underestimated the in vitro measurements.

### Load-Controlled Step

IVR values were measured against 5-Nm pure bending moment during the load-controlled step. The SFTs provided higher IVR values at the UIV level than the TRF technique for all loading directions. At the UIV level, the IVR results—normalized by the intact spine—of the TRF, MRF, and PRF models were 6.48%, 9.63%, and 12.90% for flexion (Fig. 3A), and 7.0%, 10.02%, and 13.14% for extension (Fig. 3B), respectively. For lateral bending, MRF and PRF gave 1.9 and 2.4 times higher IVR results than TRF; below the UIV level, all 3 fixation techniques gave values lower than 2.7% of the intact spine's IVR (Fig. 3C). Among all the load cases, axial rotation gave the largest normalized IVR values, with 8.76%, 44.77%, and 60.51% for TRF, MRF, and PRF, respectively (Fig. 3D).

### Displacement-Controlled Step

Maximum von Mises stress values for the screw bodies were analyzed under identical displacements for all fixa-



Unauthenticated | Downloaded 08/17/23 07:42 PM UTC

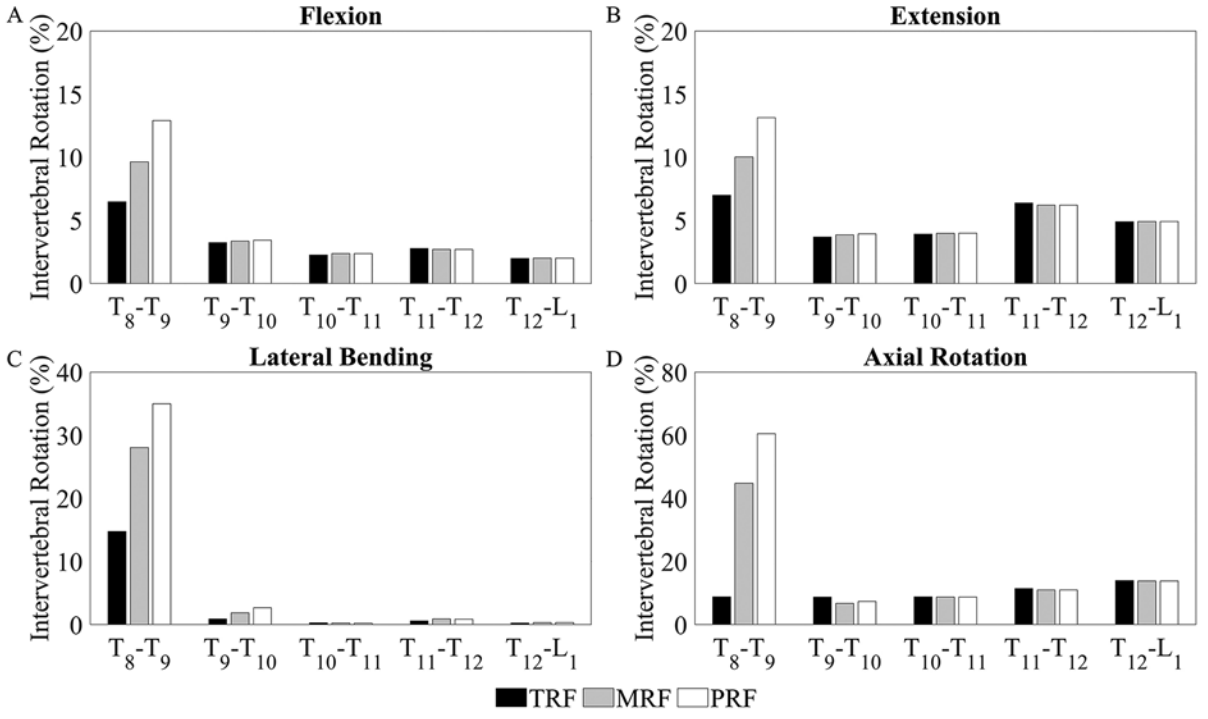


**FIG. 3.** Calculated IVR angle values, normalized for results in the intact spine, against 5-Nm pure bending moment for (**A**) flexion, (**B**) extension, (**C**) lateral bending, and (**D**) axial rotation.

tion techniques. In general, for all load directions, the TRF model provided the largest, whereas PRF gave the lowest peak stress values (Fig. 4). At the UIV level, TRF induced stress values of 37.26 MPa, 42.13 MPa, 44.4 MPa, and 44.59 MPa in flexion, extension, lateral bending, and axial rotation, respectively. In comparison to the TRF, the application of the MRF and PRF techniques reduced the maximum stress values by 17.28% and 27.72% for flexion, by 26.56% and 36.67% for extension, by 6.82% and 34.26% for lateral bending, and by 49.07% and 59.81% for axial rotation. In contrast to the other load cases, the maximum stress values below the UIV level were not reduced compared to the UIV level for axial rotation—the results were 44.59 MPa, 45.99 MPa, 46.56 MPa, 53.26 MPa, and 48.34 MPa at T8, T9, T10, T11, and T12, respectively (Fig. 4D).

### Stress Distributions

Distribution of the von Mises equivalent stress values at the UIV level was visualized and evaluated through an axial section of the FE models. In general, the largest area with stress higher than 10 MPa was found in the TRF model, whereas PRF included the smallest area with stress. The stress distributions in flexion and extension show a similar trend; i.e., the TRF technique results in much higher pedicle screw stress in both loading cases. In contrast, MRF gives less stress, whereas the PRF technique induces the least stress in both loading directions (Fig. 5A and B). For right lateral bending, the stress distribution pattern of the MRF model shows similarity with the TRF model with respect to magnitude and expansion (Fig. 5C). In contrast, for axial rotation, the peak stress values appeared at the outer edge of the screw bodies in the instrumented models, with the TRF model containing notably more area with stress above 10 MPa than the MRF and PRF models (Fig. 5D).

## Discussion

PJK remains a relatively common complication following a long instrumented posterior spinal fusion. The risk factors associated with PJK vary on an individual basis, such as older age, high body mass index, low bone mineral density, comorbidities, the surgical approach, instrumentation type, amount of deformity correction, position of the UIV, and number of vertebrae.[40–42] Previously, the sudden change in mobility was also identified as one of the risk factors, as reported by Kim et al.[43] In line with this recognition, multiple surgical procedures and instrument types have been developed to dampen this phenomenon and help the transition to normal motion at the junctional level.[8,9,13] The proposed surgical solutions include conserving the posterior ligament complex and augmentation with polymethylmethacrylate. Furthermore, the application of dynamic fixation systems or SFTs, such as TPHs, transition rods, or various types of elastic tethers or tapes, was also investigated. The current study aimed to compare the biomechanical effect of 1 rigid fixation technique and 2 different SFTs on the development of PJK after long thoracolumbar fusion.

The results of the current study highlight the fact that SFTs increase the mobility and provide a more gradual transition in motion between the instrumented and noninstrumented spinal segments. The FE method we used



Unauthenticated | Downloaded 08/17/23 07:42 PM UTC

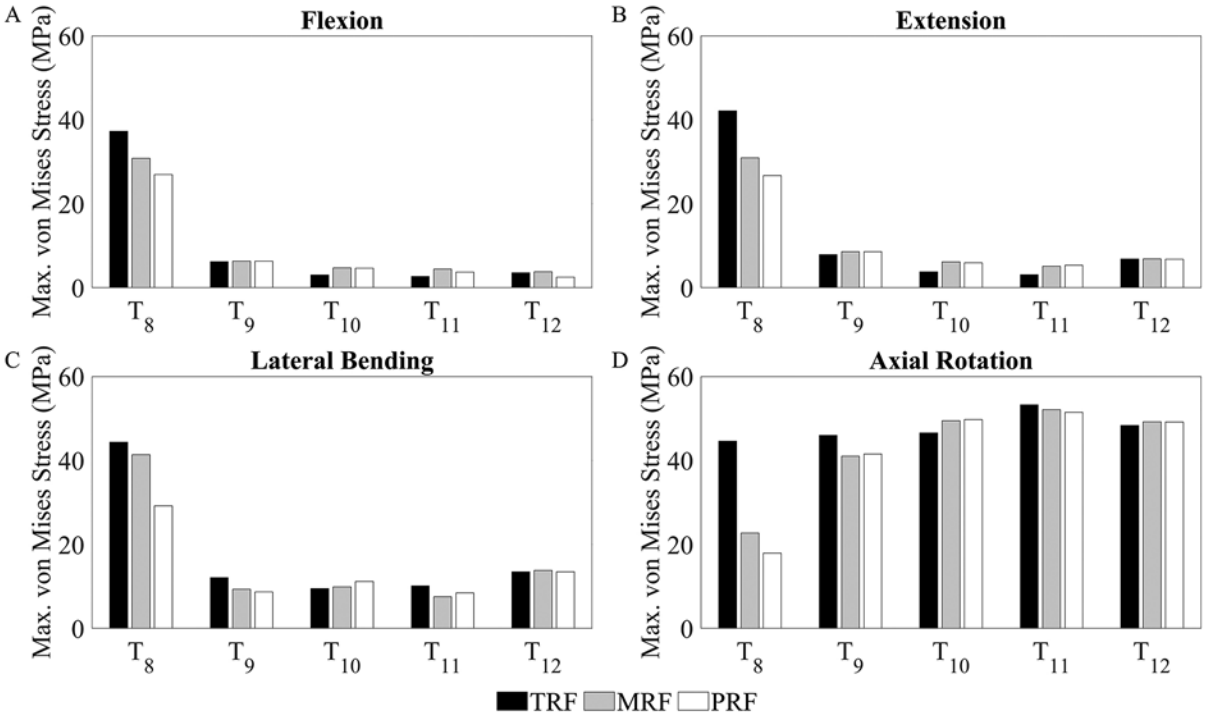


**FIG. 4.** Calculated maximum von Mises stress values on rostral pedicle screws against displacement-controlled load for (**A**) flexion, (**B**) extension, (**C**) lateral bending, and (**D**) axial rotation.

allows comparison of different techniques under identical anatomy and loading conditions, indicating that biomechanical differences are solely due to the fixation technique used.

The HD is a well-accepted and widely used criterion for evaluating the quality and accuracy of the segmentation and registration process.[44] The HD value associated with the segmentation process represents the registration quality; a lower HD value means higher accuracy.[44] The mean HD value between the lumbar and thoracolumbar L1 vertebra in the current study (minimum 0 mm, maximum 1.37 mm, mean 0.15 mm, root mean square 0.2) indicates that the registration quality is sufficient and does not compromise the results of the FE analysis.

Previous studies described the material properties of the lumbar spine region; those parameters were adopted in the current study for the whole thoracolumbar (T7–L5) spinal segment.[28,29,31–34] However, the biomechanical characteristics of the thoracic region differ from those of the lumbar spine.[38] This difference is due to the smaller IVD height, the stabilization effect of the thicker thoracic ligaments, and the presence of costovertebral joints.[38] To offset this effect, a careful calibration was performed to adjust the IVR predictions of the thoracic region to multiple experimentally obtained in vitro results.[36–38] The calibration process was accomplished by varying the weighting factor of the AF, considering the physiological limits reported in the literature.[34] The calibration resulted in a T7–L5 FE model validated against IVR and ROM of the spinal segment, and therefore suitable for further biomechanical analysis.

A modified multidirectional hybrid test protocol was used in the current study; it was introduced originally by Panjabi.[39] This loading method is particularly suitable for investigating adjacent-segment effects, because it consists of 2 successive and related loading steps. First, in the load-controlled step a pure bending moment of 5 Nm was applied to the intact and instrumented models, and then the IVR results of the intact model were used to normalize the predictions of the fixation techniques for the sake of better comparison with other investigated SFTs.[12–15] Subsequently, a displacement-controlled load was applied to the rigid technique and the 2 SFTs until the desired ROM from the first step was achieved. Although Panjabi suggested using the displacement of the intact spinal segment, corresponding values of the TRF technique were used to obtain physiologically suitable results and ensure direct comparison based on the pedicle screw load.

Our findings in the current study agree with previously published in silico and in vitro studies,[12,14] in that the SFTs allow a more gradual transition to normal motion. According to the predictions based on the current models, MRF and PRF behave less rigidly at the junctional level in all loading directions, especially in lateral bending and axial rotation. In axial rotation, the advantages of the SFTs were clearly visible; they provided substantially higher IVR values compared to the rigid technique. Similar findings were described by Doodkorte et al.[12]—namely that in axial rotation, the semirigid spinal instrumentations behave less rigidly and increase the mobility of the spinal segments at the UIV level. In lateral bending, all fixation techniques significantly limited the motions below the UIV level; thus, the role of the dampening zone increases to help the



Unauthenticated | Downloaded 08/17/23 07:42 PM UTC

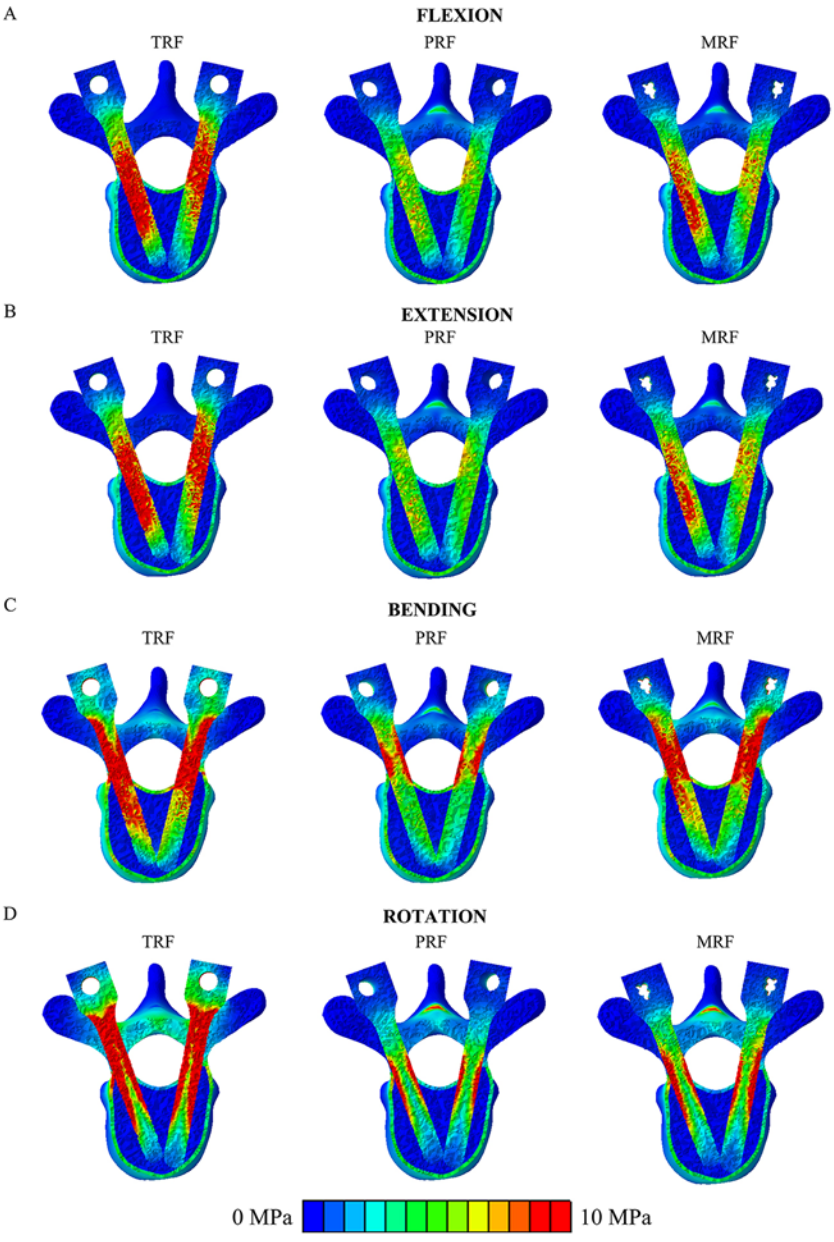


**FIG. 5.** Von Mises stress distributions of the 3 fixation techniques at the UIV level for (**A**) flexion, (**B**) extension, (**C**) right bending, and (**D**) left rotation. The maximum scale value was set to 10 MPa uniformly. Due to the symmetrical stress distribution patterns, only one direction was considered for lateral bending and axial rotation. Figure is available in color online only.

transition between the instrumented and intact segments of the spine. In addition, similar results were found in a recent cadaveric in vitro experiment by Pereira et al., who investigated the biomechanical effect of PEEK rods connected to long posterior titanium fixation.[45] They concluded that extension using PEEK rods allows redistribution of the load on the adjacent levels and decreases adjacent-level hypermobility that might be a risk factor for PJK.

The SFTs that we investigated countered the rigid technique in that a connector device was used to join the different systems. This connector itself can increase the mobility of the construct. Accordingly, to avoid biased conclusions, the effect of the connector device on mobility was investigated in Supplementary Study 1 by creating and analyzing a theoretical titanium-titanium fixation technique. The results help separate the biomechanical effects of the connector device and the fixation techniques, thus allowing appropriate conclusions. Based on the results described in Supplementary Study 1, the connector device alone does not significantly influence mobility, and the SFTs are responsible for most mobility increases and load reduction.

Pedicle screw load is an essential factor when it comes to the comparison of different fixation techniques.[14] The load of the pedicle screws indicates that the application of



Unauthenticated | Downloaded 08/17/23 07:42 PM UTC

SFTs generally reduced the maximum stresses in all fixation techniques and for all loading directions at the UIV level. It is noteworthy that below the junctional level, the maximum stress values are relatively high for axial rotation compared to other loading modes.

The ability of SFTs to reduce the pedicle stresses also has clinical implications, because it means a lower probability of vertebral compression fractures and pedicle screw pullout.[14] In addition, the decreased screw load helps prevent endplate fractures at the UIV+1 level.[14] Based on these results, using SFTs reduced the load and increased the mobility at the UIV level; hence, these SFTs contribute to the unloading of the adjacent segment and thus reduce the risk of developing PJK.

Similar to other FE analyses, the current study has some limitations worth highlighting. FE analysis is an effective tool to predict the biomechanical behaviors of anatomical structures. However, contrary to advanced biological models, it cannot address biological or physiological effects, because its calculation is based solely on mechanical theories. The results presented in our study are based on the anatomy of a healthy 24-year-old man. Our study did not consider different anatomical variations due to spinal degeneration, age, and sex. Furthermore, several simplifications in the modeling process were used because the stabilizing effects of the rib cage, the thoracic wall muscles, and costotransverse and costovertebral ligaments, as well as the effect of the upper-body weight, were not included in the current study. In order to avoid reporting unrealistic motion values originating from the listed simplifications, only normalized IVR values were included in this study. Previously published studies in the literature also considered the UIV+2 and UIV+3 levels, which were not included in the current study. Due to the static load and simplified screw geometries applied, this study cannot accurately predict the fatigue strength and the number of cycles to failure in the pedicle screws.

Despite the limitations mentioned above, the current FE analysis allowed a direct biomechanical comparison between the presented rigid and semirigid spinal fixation techniques by using identical anatomy and loading conditions. The computational model could be further developed by considering the effect of the rib cage and the muscle forces and by simulating the upper-body weight with a compressive follower load. However, we believe that the relative difference between the techniques would not change; thus, the presented results provide a satisfactory basis for comparison. However, in future work, the model could be extended rostrally to allow a more detailed biomechanical analysis at the UIV+2 and UIV+3 levels.

Based on our results, MRF and PRF techniques could reduce the risk of developing PJK after long thoracolumbar fusions. However, additional biomechanical studies and comprehensive clinical trials are recommended to analyze the clinical outcomes of these biomechanically supported load-distributing SFTs.

## Conclusions

Following long instrumented spine surgeries, the development of PJK is a frequent and clinically significant complication characterized by an unclear, multifactorial background. In the current study, FE analysis has been used to evaluate the effect of 2 SFTs compared to a conventional rigid fixation technique. In agreement with the literature, based on the findings in the current study, less rigid fixations at the rostral part of the stabilization construct allow a more gradual transition in motion between the instrumented and intact segments of the spine. Decreasing the load on the pedicle screws at the upper instrumented level could help prevent the development of PJK. However, further biomechanical and clinical studies are needed to evaluate the long-term clinical efficacy.

## Acknowledgments

Financial support from the following funding bodies is gratefully acknowledged. The project leading to the scientific results was funded by a grant from the Hungarian Scientific Research Fund, Budapest, Hungary (award no. OTKA FK123884); by the Doctoral Student Scholarship Program of the Co-operative Doctoral Program (C1014064); and by the ÚNKP-21-5 New National Excellence Program of the Ministry for Innovation and Technology—all financed from the source of the National Research, Development, and Innovation Fund. Furthermore, funding was provided by the János Bolyai Research Scholarship of the Hungarian Academy of Sciences and by the European Commission (766012-SPINNER-H2020-MSCAITN-2017).

## References

1. Good CR, Auerbach JD, O'Leary PT, Schuler TC. Adult spine deformity. *Curr Rev Musculoskelet Med*. 2011;4(4):159-167.
2. DeWald CJ, Stanley T. Instrumentation-related complications of multilevel fusions for adult spinal deformity patients over age 65: surgical considerations and treatment options in patients with poor bone quality. *Spine (Phila Pa 1976)*. 2006; 31(19)(suppl):S144-S151.
3. Glattes RC, Bridwell KH, Lenke LG, Kim YJ, Rinella A, Edwards C II. Proximal junctional kyphosis in adult spinal deformity following long instrumented posterior spinal fusion: incidence, outcomes, and risk factor analysis. *Spine (Phila Pa 1976)*. 2005;30(14):1643-1649.
4. Annis P, Lawrence BD, Spiker WR, et al. Predictive factors for acute proximal junctional failure after adult deformity surgery with upper instrumented vertebrae in the thoracolumbar spine. *Evid Based Spine Care J*. 2014;5(2):160-162.
5. Kim JS, Phan K, Cheung ZB, et al. Surgical, radiographic, and patient-related risk factors for proximal junctional kyphosis: a meta-analysis. *Global Spine J*. 2019;9(1):32-40.
6. Kim HJ, Bridwell KH, Lenke LG, et al. Patients with proximal junctional kyphosis requiring revision surgery have higher postoperative lumbar lordosis and larger sagittal balance corrections. *Spine (Phila Pa 1976)*. 2014;39(9):E576-E580.
7. Sun X, Sun W, Sun S, et al. Which sagittal evaluation system can effectively predict mechanical complications in the treatment of elderly patients with adult degenerative scoliosis? Roussouly classification or Global Alignment and Proportion (GAP) Score. *J Orthop Surg Res*. 2021;16(1):641.
8. Bylski-Austrow DI, Glos DL, Bonifas AC, Carvalho MF, Coombs MC, Sturm PF. Flexible growing rods: a biomechanical pilot study of polymer rod constructs in the stability of skeletally immature spines. *Scoliosis Spinal Disord*. 2016; 11(1):39.
9. Thawrani DP, Glos DL, Coombs MT, Bylski-Austrow DI, Sturm PF. Transverse process hooks at upper instrumented vertebra provide more gradual motion transition than pedicle screws. *Spine (Phila Pa 1976)*. 2014;39(14):E826-E832.
10. Cahill PJ, Wang W, Asghar J, et al. The use of a transition



Unauthenticated | Downloaded 08/17/23 07:42 PM UTC

rod may prevent proximal junctional kyphosis in the thoracic spine after scoliosis surgery: a finite element analysis. *Spine (Phila Pa 1976)*. 2012;37(12):E687-E695.
11. Gornet MF, Chan FW, Coleman JC, et al. Biomechanical assessment of a PEEK rod system for semi-rigid fixation of lumbar fusion constructs. *J Biomech Eng*. 2011;133(8):081009.
12. Doodkorte RJP, Roth AK, Arts JJ, Lataster LMA, van Rhijn LW, Willems PC. Biomechanical comparison of semirigid junctional fixation techniques to prevent proximal junctional failure after thoracolumbar adult spinal deformity correction. *Spine J*. 2021;21(5):855-864.
13. Viswanathan VK, Ganguly R, Minnema AJ, et al. Biomechanical assessment of proximal junctional semi-rigid fixation in long-segment thoracolumbar constructs. *J Neurosurg Spine*. 2018;30(2):184-192.
14. Bess S, Harris JE, Turner AWL, et al. The effect of posterior polyester tethers on the biomechanics of proximal junctional kyphosis: a finite element analysis. *J Neurosurg Spine*. 2017; 26(1):125-133.
15. Zhang M, Ren W, Mo Z, Li J, Pu F, Fan Y. Biomechanics of adjacent segment after three-level lumbar fusion, hybrid single-level semi-rigid fixation with two-level lumbar fusion. *Comput Methods Biomech Biomed Engin*. 2022;25(4):455-463.
16. Farkas J, Varga PP, inventors. Set of surgical instruments for the fixation of vertebrae. European patent WO2002041797A1. May 30, 2002.
17. Aryanto KYE, Oudkerk M, van Ooijen PMA. Free DICOM de-identification tools in clinical research: functioning and safety of patient privacy. *Eur Radiol*. 2015;25(12):3685-3695.
18. Cignoni P, Rocchini C, Scopigno R. Metro: measuring error on simplified surfaces. *Comput Graph Forum*. 1998;17(2):167-174.
19. Shirazi-Adl SA, Shrivastava SC, Ahmed AM. Stress analysis of the lumbar disc-body unit in compression. A three-dimensional nonlinear finite element study. *Spine (Phila Pa 1976)*. 1984;9(2):120-134.
20. Baroud G, Nemes J, Heini P, Steffen T. Load shift of the intervertebral disc after a vertebroplasty: a finite-element study. *Eur Spine J*. 2003;12(4):421-426.
21. Remus R, Lipphaus A, Neumann M, Bender B. Calibration and validation of a novel hybrid model of the lumbosacral spine in ArtiSynth—the passive structures. *PLoS One*. 2021; 16(4):e0250456.
22. Zeng ZL, Zhu R, Wu YC, et al. Effect of graded facetectomy on lumbar biomechanics. *J Healthc Eng*. 2017;2017:7981513.
23. White AA, Panjabi MM. *Clinical Biomechanics of the Spine*. Lippincott; 1990.
24. Park WM, Kim K, Kim YH. Effects of degenerated intervertebral discs on intersegmental rotations, intradiscal pressures, and facet joint forces of the whole lumbar spine. *Comput Biol Med*. 2013;43(9):1234-1240.
25. Rohlmann A, Burra NK, Zander T, Bergmann G. Comparison of the effects of bilateral posterior dynamic and rigid fixation devices on the loads in the lumbar spine: a finite element analysis. *Eur Spine J*. 2007;16(8):1223-1231.
26. Lu Y, Rosenau E, Paetzold H, et al. Strain changes on the cortical shell of vertebral bodies due to spine ageing: a parametric study using a finite element model evaluated by strain measurements. *Proc Inst Mech Eng H*. 2013;227(12):1265-1274.
27. Noailly J, Wilke HJ, Planell JA, Lacroix D. How does the geometry affect the internal biomechanics of a lumbar spine bi-segment finite element model? Consequences on the validation process. *J Biomech*. 2007;40(11):2414-2425.
28. Rohlmann A, Bauer L, Zander T, Bergmann G, Wilke HJ. Determination of trunk muscle forces for flexion and extension by using a validated finite element model of the lumbar spine and measured in vivo data. *J Biomech*. 2006;39(6):981-989.
29. Li J, Shang J, Zhou Y, Li C, Liu H. Finite element analysis of a new pedicle screw-plate system for minimally invasive transforaminal lumbar interbody fusion. *PLoS One*. 2015; 10(12):e0144637.
30. Rohlmann A, Zander T, Schmidt H, Wilke HJ, Bergmann G. Analysis of the influence of disc degeneration on the mechanical behaviour of a lumbar motion segment using the finite element method. *J Biomech*. 2006;39(13):2484-2490.
31. Shirazi-Adl A, Ahmed AM, Shrivastava SC. Mechanical response of a lumbar motion segment in axial torque alone and combined with compression. *Spine (Phila Pa 1976)*. 1986; 11(9):914-927.
32. Finley SM, Brodke DS, Spina NT, DeDen CA, Ellis BJ. FE-Bio finite element models of the human lumbar spine. *Comput Methods Biomech Biomed Engin*. 2018;21(6):444-452.
33. Schmidt H, Heuer F, Drumm J, Klezl Z, Claes L, Wilke HJJ. Application of a calibration method provides more realistic results for a finite element model of a lumbar spinal segment. *Clin Biomech (Bristol, Avon)*. 2007;22(4):377-384.
34. Schmidt H, Heuer F, Simon U, et al. Application of a new calibration method for a three-dimensional finite element model of a human lumbar annulus fibrosus. *Clin Biomech (Bristol, Avon)*. 2006;21(4):337-344.
35. Wilke HJ, Wenger K, Claes L. Testing criteria for spinal implants: recommendations for the standardization of in vitro stability testing of spinal implants. *Eur Spine J*. 1998;7(2): 148-154.
36. Rohlmann A, Neller S, Claes L, Bergmann G, Wilke HJ. Influence of a follower load on intradiscal pressure and intersegmental rotation of the lumbar spine. *Spine (Phila Pa 1976)*. 2001;26(24):E557-E561.
37. Couvertier M, Germaneau A, Saget M, et al. Biomechanical analysis of the thoracolumbar spine under physiological loadings: experimental motion data corridors for validation of finite element models. *Proc Inst Mech Eng H*. 2017;231(10):975-981.
38. Wilke HJ, Herkommer A, Werner K, Liebsch C. In vitro analysis of the segmental flexibility of the thoracic spine. *PLoS One*. 2017;12(5):e0177823.
39. Panjabi MM. Hybrid multidirectional test method to evaluate spinal adjacent-level effects. *Clin Biomech (Bristol, Avon)*. 2007;22(3):257-265.
40. Park SJ, Lee CS, Chung SS, Lee JY, Kang SS, Park SH. Different risk factors of proximal junctional kyphosis and proximal junctional failure following long instrumented fusion to the sacrum for adult spinal deformity: survivorship analysis of 160 patients. *Neurosurgery*. 2017;80(2):279-286.
41. Diebo BG, Jalai CM, Challier V, et al. Novel index to quantify the risk of surgery in the setting of adult spinal deformity: a study on 10,912 patients from the Nationwide Inpatient Sample. *Clin Spine Surg*. 2017;30(7):E993-E999.
42. Kim DK, Kim JY, Kim DY, Rhim SC, Yoon SH. Risk factors of proximal junctional kyphosis after multilevel fusion surgery: more than 2 years follow-up data. *J Korean Neurosurg Soc*. 2017;60(2):174-180.
43. Kim YJ, Bridwell KH, Lenke LG, Kim J, Cho SK. Proximal junctional kyphosis in adolescent idiopathic scoliosis following segmental posterior spinal instrumentation and fusion: minimum 5-year follow-up. *Spine (Phila Pa 1976)*. 2005; 30(18):2045-2050.
44. Karimi D, Salcudean SE. Reducing the Hausdorff distance in medical image segmentation with convolutional neural networks. *IEEE Trans Med Imaging*. 2020;39(2):499-513.
45. Pereira BA, Lehrman JN, Sawa AGU, et al. Biomechanical effects of proximal polyetheretherketone rod extension on the upper instrumented and adjacent levels in a human long-segment construct: a cadaveric model. *Neurospine*. 2022;19(3): 828-837.

## Disclosures

Dr. Lazary is a patent holder with Sanatmetal Ltd.



Unauthenticated | Downloaded 08/17/23 07:42 PM UTC

## Author Contributions

Conception and design: Eltes, Turbucz, Varga, Lazary. Acquisition of data: Turbucz, Fayad. Analysis and interpretation of data: Eltes, Turbucz, Pokorni, Varga, Lazary. Drafting the article: Turbucz, Fayad. Critically revising the article: all authors. Reviewed submitted version of manuscript: all authors. Approved the final version of the manuscript on behalf of all authors: Eltes. Study supervision: Eltes, Lazary. Figures: Eltes, Turbucz, Pokorni.

## Supplemental Information

### Online-Only Content

Supplemental material is available with the online version of the article.

*Supplementary Materials*. https://thejns.org/doi/suppl/10.3171/2023.1.SPINE22931.

## Correspondence

Peter E. Eltes: Semmelweis University, Budapest, Hungary. eltespeter@yahoo.com.



Unauthenticated | Downloaded 08/17/23 07:42 PM UTC